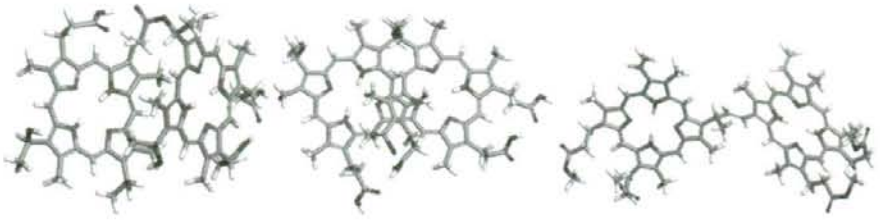

(a) (b) (c)

Fig. 2 Optimized structures of: (a) Ester linked; (b) Ether linked; and (c) the C-C linked dimers.

dynamic therapy, particular attention was devoted to two spectral aspects that are important for an ideal photosensitizer: (1) determination of the energetic gap between singlet and triplet excited states, shows that the values are greater than 0.98 eV and (2) computation of the Q-band absorption maximum shows that they have weaker transitions with low oscillator strength. Among the dimers C–C linked dimer has higher oscillator strength. Thus dimers may involve in the PDT activity, when used at higher dosage.

Acknowledgement

Grant support: Grants-in-aid for Research Project; Promotion of Advanced Medical Technology (H18-Nano-001); Ministry of Health, Labour and Welfare of Japan is gratefully acknowledged. R.V.B. thanks the Ministry of Education, Culture, Sports, Science and Technology of Japan (Grant No. 17686072) for financial support. The authors are also grateful to the staff of CCMS, IMR, and Tohoku University for computational support.

REFERENCES

1) I. J. MacDonald and T. J. Dougherty: J. Porphyrins Phthalocyanines. **5** (2001) 105–129.
2) Y. Van Tenten, H. J. Schuitmaker, A. De Wolf, B. Willekens, G. F. J. M. Vrensen and M. J. Tassignon: Exp. Eye Res. **72** (2001) 41–48.
3) T. J. Dougherty, C. J. Gomer, B. W. Henderson, G. Jori, D. Kessel, M. Korbelik, J. Moan and Q. Peng: J. Natl. Cancer Inst. **90** (1998) 889–905.
4) C. Avendano and J. Carlos Menendez: *Medicinal chemistry of anticancer drugs* (Elsevier's Science & Technology Rights, Department in Oxford, UK, 2008) pp. 93–132.
5) R. Bonnett: Chem. Soc. Rev. **24** (1995) 19–33.
6) R. K. Pandey and G. Zheng: *Porphyrins as Photosensitizers in Photodynamic Therapy*, vol. 6. (Academic Press: San Diego, 2000).
7) M. R. Detty, S. L. Gibson and S. J. Wagner: J. Med. Chem. **47** (2004) 3897–3915.
8) M. M. Siegel, K. Tabei and R. Tsao: J. Mass. Spectrom. **34** (1999) 661–669.
9) K. M. Kadish, K. M. Smith and R. Guilard: *The Prophyrin Handbook* (Academic New York, 1978) pp. 189–190.
10) B. W. Henderson, D. A. Bellnier, W. R. Greco, A. Sharma, R. K. Pandey, L. A. Vaughan, K. R. Weishaupt and T. J. Dougherty: Cancer Res. **57** (1997) 4000–4007.
11) R. J. Deeth: Faraday Discuss **124** (2003) 379–391.
12) V. N. Nemykin, R. G. Hadt, R. V. Belosludov, H. Mizuseki and Y. Kawazoe: J. Phys. Chem. A **111** (2007) 12901–12913.
13) Gaussian 03, Revision C.02, M. J. Frisch, *et al.* Gaussian, Inc., Wallingford 2003.
14) K. A. Nguyen and R. Pachater: J. Chem. Phys. **114** (2001) 10757–40767.
15) C. J. Byrne, L. M. Marshallsay and A. D. Ward: J. Photochem. Photobiol. **6** (1990) 13–27.
16) C. J. Byrne, M. A. Cooper, P. A. Cowled, R. A. W. Johnstone, L. Mackenzie, L. V. Marshallsay, I. K. Morris, C. A. Muldoon, M. J. Raftery, S. S. Yin and A. D. Ward: Aust. J. Chem. **57** (2004) 1091–1102.
17) C. J. Byrne and A. D. Ward: Aust. J. Chem. **44** (1991) 411–426.
18) R. K. Pandey, J. F. Majchrzycki, K. M. Smith and T. J. Dougherty: Proc. SPIE. **1065** (1989) 164–174.
19) N. J. Turro: *Singlet oxygen and chemiluminescent organic reactions, Modern Molecular Photochemistry*, (University Science Books: California, 1991) pp. 583–593.

EXPERIMENTAL CELL RESEARCH 314 (2008) 3563–3569

available at www.sciencedirect.com

ScienceDirect

www.elsevier.com/locate/yexcr

Research Article

Intracellular imaging of targeted proteins labeled with quantum dots

Jungwoo Yoo[a,1], *Taketoshi Kambara*[b,2], *Kohsuke Gonda*[b,3], *Hideo Higuchi*[b,2,*]

[a]*Department of Material Science, Graduate School of Engineering, Tohoku University, Sendai, Japan*
[b]*Biomedical and Engineering Research Organization, Tohoku University, Sendai, Japan*

ARTICLE INFORMATION

Article Chronology:
Received 17 July 2008
Revised version received
5 September 2008
Accepted 7 September 2008
Available online 26 September 2008

Keywords:
Motor protein
Actin
Microtubule
Kinesin
Quantum dots
Microscope
Imaging

ABSTRACT

We developed a new method for imaging the movement of targeted proteins in living cancer cells with photostable and bright quantum dots (QDs). QDs were conjugated with various molecules and proteins, such as phalloidin, anti-tubulin antibody and kinesin. These bioconjugated QDs were mixed with a transfection reagent and successfully internalized into living cells. The movements of individual QDs were tracked for long periods of time. Phalloidin conjugated QDs bound to actin filaments and showed almost no movement. In contrast, anti-tubulin antibody conjugated QDs bound to microtubules and revealed dynamic movement of microtubules. Kinesin showed an interesting behavior whereby kinesin came to be almost paused briefly for a few seconds and then moved once again. This is in direct contrast to the smoothly continuous movement of kinesin in an *in vitro* assay. The maximum velocity of kinesin in cells was faster than that in the *in vitro* assay. These results suggest that intracellular movement of kinesin is different from that in the *in vitro* assay. This newly described method will be a powerful tool for investigating the functions of proteins in living cells.

Introduction

Recent development of imaging techniques for single molecules provides detailed information of the molecular mechanism of proteins [1–4]. However, the mechanism underlying the function of these molecules within the cells is still not known. Many studies of cell biology are utilizing organic fluorophores and fluorescence proteins, such as Cy3 and GFP, as probes to visualize single protein molecules, and have been very successful [5,6]. Single molecule observation of these fluorophores, however, is available only for short periods of a few seconds due to their rapid photo bleaching. Thus, development of a new technique to image single molecules of targeted proteins for long periods of time is crucial in order to investigate the detailed mechanisms of the proteins in living cells. The bright and photostable quantum dots (QDs) are useful for detecting the behavior of biomolecules in living cells for long periods of time [7–11], 1 h or longer [10]. The positions of bright fluorescence spots were determined with more than one nanometer accuracy for the long periods, when the QDs are excited with very bright light [12,13]. Thus, the direct labeling of biomolecules in a living cell with QDs is important for the future advances of biological and medical research [12,14,15].

* *Corresponding author.* Department of Physics, Graduate School of Science, University of Tokyo, Hongo Bunkyo-ku Tokyo, Japan 113-8654. Fax: +81 35841 7646.
E-mail address: higuchi@phys.s.u-tokyo.ac.jp (H. Higuchi).
[1] Institute of Multidisciplinary Research for Advanced Materials, Tohoku University, 2-1-1, Katahira, Aoba-ku, Sendai 980-8577, Japan.
[2] Department of Physics, Graduate School of Science, the University of Tokyo, Hongo Bunkyou-ku Tokyo 113-8654, Japan.
[3] Department of Nano-Medical Science, Graduate School of Medicine, Tohoku University, Seiryo-machi, Aoba-ku, Sendai 980-8574, Japan.

0014-4827/$ – see front matter © 2008 Elsevier Inc. All rights reserved.
doi:10.1016/j.yexcr.2008.09.014

Internalization of the QD-bioconjugates across the cell membrane into cytoplasm of living cells is very challenging for intracellular imaging. Several methods for the internalization of QD-bioconjugates have been tested, electroporation [16], liposome fusion [17,18], microinjection [17] and cell penetrating polymers and peptides [19,20]. These methods, however, could internalize QDs in aggregates [17,18]. To image single molecules labeled with QDs in living cells, the bioconjugated QDs need to be delivered in a monodispersion and have increased targeting efficiency. Recently, osmotic lysis of pinosomes was used for QD internalization [21]. This method is simple but has sometimes resulted in damage of cellular functions [22].

Our method using the lipid transfection has been widely used for DNA transfection in cell biology [23] to deliver QDs into cells without damaging cellular functions. We successfully delivered the bioconjugated QDs and imaged them internally using QDs conjugated with phalloidin, anti-tubulin antibody and kinesin as excellent examples of small molecule, antibody and enzyme, respectively (Fig. 1). Here, the interesting dynamics of microtubule and the intracellular-specific behavior of kinesin were discovered for the first time. Therefore, the methods in the present study will be a powerful tool to image other cellular components as well as motor proteins using photostable QDs as a probe.

Materials and methods

Preparation of phalloidin–QD-bioconjugate

For the specific labeling of actin filaments, phalloidin molecules were conjugated to QDs. Amino functionalized PEG coated QDs 655 (Qdot® nanocrystals, Invitrogen Co.), where the number indicates the emission wavelength, were cross-linked to amino functionalized phalloidin (Amino Phalloidin, Alexis Biochemicals) by Bis (sulfosuccinimidly) suberate (BS3, Pierce Chemicals). BS3 is a homobifunctional *N*-hydroxysuccinimide ester (NHS ester) that reacts efficiently with primary amino groups. The procedure to make phalloidin conjugated QDs is described as follows: 0.03 mg of BS3 was added to 50 μl of 4 μM QD solution and incubated for 30 min at room temperature (~25 °C). Excess cross-linker was removed by NAP-5 column (Amersham Biosciences) with PBS (pH 7.4). 6 μg of amino-phalloidin was then added to the solution, and incubated for 2 h with gently mixing at room temperature. To remove the free phalloidin, a 100 kDa ultrafiltration filter (Nanosep, Pall Life Sciences) was used according to manufacturer instructions. The phalloidin–QDs were resuspended in phosphate buffered saline, PBS (pH 7.4) and stored at 4 °C. The final concentration of phalloidin–QDs was determined by measuring the absorbance of the conjugate solution.

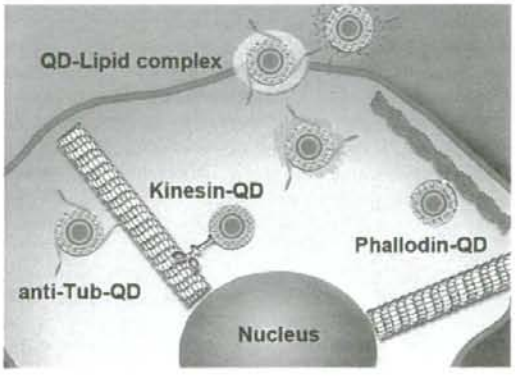

Fig. 1 – A schematic diagram of our intracellular imaging technique. QD–lipid complexes were internalized by the fusion of cellular membrane. Various bioconjugated QDs entered into cytoplasm and the bioactivities were retained in the cells. Phalloidin–QDs and anti-tubulin–antibody–QDs specifically bound to the actin filaments and the microtubules, respectively. Kinesin-QDs moved on the microtubules.

Antibody–QD conjugate

To label microtubules in the living cells, QDs were conjugated to a monoclonal antibody against microtubules. Amino functionalized PEG coated QD 655 (Qdot® nanocrystals, Invitrogen Co.) was linked to anti-bovine α-tubulin mouse monoclonal antibody (isotype IgG1, Molecular Probes). Qdot® Antibody Conjugation Kit (Qdot® nanocrystals, Invitrogen) was used according to manufacturer instructions. The anti-tubulin–QDs were suspended in PBS (pH 7.4) and stored at 4 °C. The final concentration of anti-tubulin–QDs was determined by measuring the absorbance of QDs in the conjugate solution.

Kinesin–QD conjugate

Kinesin-1, 560 amino acids with biotin-tag at C-terminal, from mouse (KIF-5a) was linked to QDs via the streptavidin–biotin reaction. Streptavidin functionalized PEG coated QD 655 (Qdot® nanocrystals, Invitrogen) was conjugated to C-terminal biotinylated kinesin. 5 μl of 1 μM QD solution was diluted by 5 μl of PBS (pH 7.4). Then 30 μl of 1 μM kinesin solution was added to the QD solution and incubated for 20 min at room temperature. The kinesin–QDs were stored at 4 °C.

Internalization of QD-bioconjugates into living cells

Assemblies of QD–lipid complexes were prepared as follows. The bioconjugated QD solution was diluted with 97 μl of serum-free L-15 medium (GIBCO, Invitrogen Co.) to 5 nM, and then 3 μl of lipid reagent (FuGENE® HD, Roche Ltd.) was added directly into the medium containing the diluted QD-bioconjugates. The solution was tapped for mixing, and incubated for 20 min at room temperature. For treatment with the QD–lipid complex, human breast cancer cells, MDA-MB-231 (ATCC Co.), were grown in a glass-bottom dish with L-15 medium containing 10% FBS. The cells were washed with FBS-free L-15 medium, and the culture medium was then exchanged with 1 ml of the FBS-free L-15 medium. The QD–lipid complex was added to the cells (with final concentration of 0.5 nM) and incubated for 3 h. After 3 h of incubation, the cells were washed with PBS buffer to remove the non-binding QD–lipid complex, and then 2 ml of L-15 medium with 10% FBS was added. Observations commenced 2 h after this final addition.

All internalization procedures were performed at 37 °C in an incubator and observed at 35 °C on the microscope except in the QD–kinesin conjugates experiment. In this latter case the QD–kinesin–lipid complex incubation in cells was performed at 27 °C

in FBS-free L-15 medium that contained 1 mM ATP. Observations were performed at 25 °C.

Optical system with confocal microscope

The optical system for two-dimensional observations of fluorescence from QDs consisted primarily of an epi-fluorescent microscopy (IX-71, Olympus) with modifications, a Nipkow disk type confocal unit (CSU 10, Yokogawa), and an electron multiplier type charge-coupled device camera (EM-CCD, Ixon DV887, Andor Technology) [13]. The objective lens (100× UPlanFLN, 1.30 NA, oil, Olympus) was used for phase contrast imaging. QDs were illuminated by a green laser (532 nm wavelength, Crystalaser). The fluorescence from the QDs was filtered (transmission wavelength of the filter was >580 nm; Omega Optics, Austin). Images were taken with the rate of 10 to 30 frames per second.

MSD analysis of single particle movement

To investigate the dynamic behavior of a particle, Mean Square Displacement (MSD) was calculated from x–y coordinates of individual tracking position data [24]. MSD values of individual tracking are defined by the following equation.

$$\mathrm{MSD}(n\Delta t) = \frac{1}{N-n}\sum_{i=1}^{N-n}\left[(x_{i+n}-x_i)^2+(y_{i+n}-y_i)^2\right]$$

where x_i and y_i are positions on frame i, N is the total number of frames. Δt is the time between frames and distance between steps in time t and $n\Delta t$ is the time interval over which the MSD is calculated. Thus MSD is a function of time. To get the information for the diffusion coefficients and the velocities, MSD were fitted by the following equation.

$$\mathrm{MSD}(\Delta t) = 4D\Delta t + V^2(\Delta t)^2 \qquad \lim_{t\to 0}\mathrm{MSD}(\Delta t) = 4D\Delta t$$

where D is diffusion coefficient and V is drift velocity.

When MSD was fitted versus time, the linear plot of MSD produced represents random Brownian movement. When the change in MSD was nonlinear with time, the movement is directed diffusion or confined diffusion. A decreasing slope indicates confined movement. On the other hand, directed diffusion produces an MSD plot with an increasing slope.

Results and discussion

We developed a lipid transfection based delivery method using the transfection reagent, FuGENE® HD. We tested the best condition to introduce QDs without aggregation into cells. The ratio of QD and the FuGENE concentrations is important to deliver many single QDs in cells. Although the higher concentration of FuGENE delivers many QDs into living cells, it is harmful to living cells. Thus the concentration of FuGENE is fixed according to manufacturer instructions, and then various concentrations of QDs were tested to find the best condition for delivery of a lot of single QDs into living cells. The criteria for single QDs without aggregation is that the fluorescence intensity of QD at on-state of blinking [10,13] is within 0.7–1.3 times of single quantum dot intensity measured before mixing with FuGENE. Based on this criteria, we tested three conditions that 97 μl of the 1.5, 5 and 12 nM QD solution mixed with 3 μl of the transfection reagent, and this mixture was diluted 10 times with adding 900 μl of L-15 medium before adding it to the cells (detailed see Materials and Methods). At QD concentration of 12 nM, aggregation of QDs was increased. At QD concentration of 1.5 nM, QD keeps single particle but less number of QDs were internalized. The best condition was obtained at 5 nM QD solution. This was the same to all of types of bioconjugated QDs tested. We have delivered hundreds (100–400) of non-conjugated QDs into a single living cell with the best condition.

The non-conjugated QDs were observed under a Nipkow disk confocal microscope [13]. Hundreds of QDs were delivered into cytoplasm of living cells (Figs. 2A and B) and imaged for 10 min or longer. Their position in living cells was tracked using a previously described single molecule tracking method [13]. Single QDs were moved by random diffusion (Fig. 2B right panel) and they did not aggregate around the nucleus region. The delivered QDs were successfully dispersed as single QDs without forming aggregations in the cytoplasm unlike previous reports [17,18]. This is also in direct contrast to the endocytosis based delivery method of QDs where the QDs formed aggregates in perinucleus region [13,17,25]. These results indicate that the non-conjugated QDs were delivered in cytoplasm without using any coatings such as a vesicle and their movements in the cytoplasm were by diffusion.

To determine if this method could deliver bioconjugated-QDs into cells, we attempted to deliver QDs conjugated with small molecules of phalloidin which specifically bound to the actin filaments. The amino QD655 was specifically cross-linked with amino-phalloidin. Phalloidin–QDs were inserted into the living cells and observed specifically underneath the cell membrane where actin filaments are localized [13] (Fig. 2C upper panel). Tracking of these phalloidin–QDs showed almost no movement even when measurements were taken for 30 s. This is in direct contrast to the random movement of the non-conjugated QDs.

To confirm the specific colocalization of phalloidin–QD conjugates with actin filaments, the cells were treated with cytochalasin D which depolymerizes actin filaments. After 10 min treatment with cytochalasin D, phalloidin–QDs moved randomly with similar movements to non-conjugated QDs (see Supporting information, Fig. S1). We further analyzed quantitatively the dynamics of phalloidin–QDs by cytochalasin D treatment (Fig. S2). Phalloidin–QDs before (79 QDs) and after (93 QDs) cytochalacin D treatment were tracked with video rate of 33 ms and then their average velocities within 10 s were calculated. After 10 min of treatment with Cytochalacin D, the velocities of the half of the QDs were increased. These results indicate that phalloidin–QDs bound to immobile actin filaments become free to move after treatment with cytochalasin D.

A mean square displacement (MSD) analysis was performed to qualitatively measure the overall motion of the QDs including diffusion and directed movement [14,24] as seen in Fig. 3.

The plots of non-conjugated and phalloidin–QDs could be fitted to a linear line representing the diffusion coefficient of random diffusion. The diffusion coefficient for non-conjugated-QDs (n=211 in 4 cells) was 3180 nm^2/s, which is approximately 8 times faster than that of the phalloidin–QDs, 410 nm^2/s. The diffusion coefficients of phalloidin–QD (n=353 in 4 cells) increased when the cell was treated by cytochalacin D. After a 10 min treatment, the diffusion coefficient was 2550 nm^2/s (Fig. S3), which is similar to that of non-conjugated-QDs. This indicates that complexes of

phalloidin–QDs and actin filaments had been released. These results confirm that our intracellular delivery method can indeed be used for specific labeling of living cellular components.

Antibody based imaging is the one of popular methods for specific targeting of various proteins. To test the potential of our intracellular targeting method in wider applications, we attempted to deliver antibody conjugated QDs that bind to targeted cellular components. Microtubules were specifically targeted because they play an important role in a structural support as part of the cytoskeleton and have dynamic behaviors such as polymerization and depolymerization [26]. To label microtubules, QDs were linked to anti α-tubulin antibody (anti-tubulin–QD) which has a specific affinity to a tubulin dimer in the microtubule filaments. Hundreds of the anti-tubulin–QD conjugates delivered to the cell were spread throughout the entire cell cytoplasm (Fig 2D). This is in contrast with phalloidin–QD conjugates which were detected only in the peripheral areas of the cell. Remarkably, the linear traces could be clearly observed when QDs were exposed for 30 s (Figs. 2D and S3). The anti-tubulin–QDs moved directionally with backward and forward movements. The directional movement was supported by MSD plot (n=76 in 3 cells) (Fig. 3). The MSD plot of anti-tubulin–QDs could be fitted to parabolic curves indicating directional movement with an average value of 50.3 nm/s. This is in direct contrast to non-conjugated QDs and phalloidin–QDs. These results also support the directional movement of

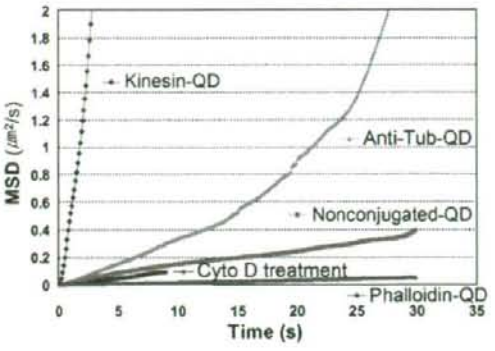

Fig. 3 – MSD plots of various bioconjugated QDs. While non-conjugated-QDs show the linear plot indicative of a random diffusion with D=3180 nm²/s (linear fitting with R^2=0.968), phalloidin–QDs indicate the slow movement of actin filaments (D=410 nm²/s, R^2=0.994). In the 10 min treatment of cytochalasin D, the diffusion coefficient of phalloidin–QDs became to the random diffusion, D=2550 nm²/s (R^2=0.9677, observation in 33 ms, video rate). The MSD plots of kinesin–QDs and anti-tubulin–QDs exhibit the directional movement in their dynamic behaviors by increasing their slopes. The average velocities calculated from the curve were 457 nm/s for kinesin (R^2=0.962), and 50.3 nm/s for microtubules (R^2=0.972).

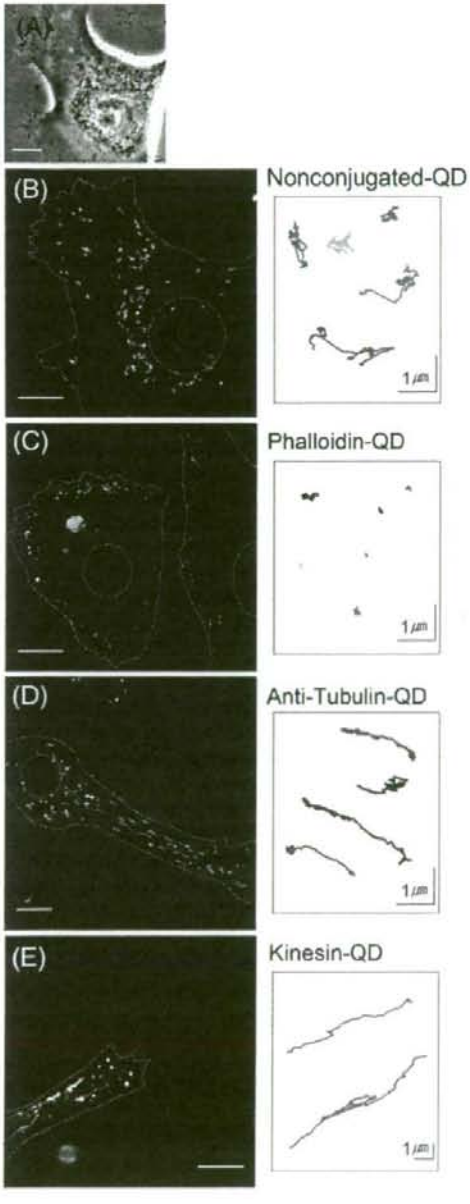

Fig. 2 – Intracellular delivery of the various types of bioconjugated QDs in living cells. (B)–(E) Left panels are the fluorescence images of QDs with a 0.1 s exposure time. Blue line is the trajectory of each QD for 30 s and the orange dotted line represents the cell membrane and nucleus. Right panels are the magnified views of each trajectory. (A) Phase contrast image of the living cell of (B) as a fluorescence image. (B) Fluorescence image of non-conjugated-QDs. The trajectories in the right panel had a random shape. (C) Trajectories of phalloidin–QDs. They showed the specific binding to actin filaments. (D) Trajectories of anti-tubulin-QDs. The trajectories displayed the dynamics of microtubules. (E) Fluorescence image of kinesin-QDs. The linear trajectories were indicative of directed motions of kinesin motors. White scale bars, 10 μm.

microtubules. The directional movement possibly derives from the dynamics of microtubules [26].

If QDs are delivered not by the intracellular delivery but by endocytosis, they still exhibit directional movement towards the nucleus region by vesicle transport on the microtubules [13,27]. Thus it is critical to determine whether the QDs were binding to microtubules or being transported in vesicles. To confirm the QDs were specifically targeting microtubules, cells were incubated with anti-tubulin–QD conjugates for 30 h. This provided sufficient time for endocytosed QDs to aggregate in the perinucleus region by motor protein transport [13]. However, after this long incubation time, the QDs did not form aggregates around the nucleus. Instead, they remained dispersed throughout the cell cytoplasm specifically binding to the microtubules (Fig. S4). This result indicates that the antibody–QD conjugates had been delivered into the cytoplasm without any coating and they retained their ability to bind to specific target proteins in the living cells.

In order to demonstrate how powerful our intracellular delivery method is, we delivered purified motor protein-conjugated QDs into the cytoplasm and traced the movement of QDs to investigate behavior of a purified protein in living cells. Avidin–QDs were conjugated to a biotinylated recombinant motor protein, kinesin-1, using an avidin–biotin coupled reaction. Kinesin walks along a microtubule from its minus to plus end in a living cell [3]. Kinesin–QD conjugates were incubated with the lipid reagent and added to the cultured cells. Similar to the other conjugates, kinesin–QD conjugates did not form large aggregations, instead they were spread evenly throughout the cytoplasm. Fig. 2E shows the results for single particle tracking of kinesin–QDs. The majority of the QDs were moving in these images. As expected, kinesin–QDs moved both linearly and directionally. Detail analysis, however, revealed QDs exhibited stop and back movements along the same track (Fig. 2E). Using the *in vitro* motility assays on a cover slip [3,28,29], purified kinesin moved smoothly and continuously along microtubules in contrast to irregular movement of kinesin in cell as discussed later. This suggests that there must be unknown factors that regulate the intracellular movement of kinesin in living cells.

The movements of kinesin–QD were analyzed using a MSD method (Fig. 3). The plots (n=20 in 5 cells) were well fitted to parabolic curves, indicating directional movement towards the cell membrane driven by kinesin. The average velocity of kinesin that

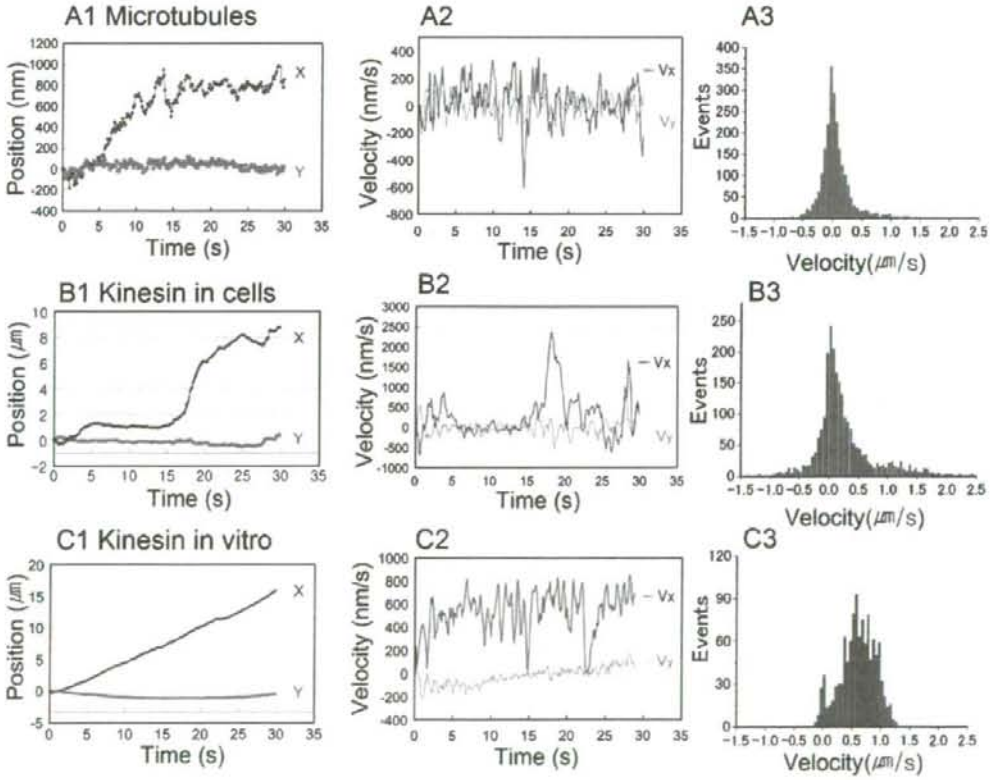

Fig. 4 – Trajectory analysis of the dynamics of (A) microtubules, (B) kinesin in cells and (C) kinesin *in vitro*. First column is the *x*, *y* position plots versus time. It exhibits the directionality in the *X* axis (transverse direction of microtubule filament). Second column is the plot of the velocity in the *X* (V_x) and *Y* axes (V_y). The third column is the *X* axis velocity (V_x) distributions of (A) microtubules, (B) kinesin in cells and (C) kinesin *in vitro*. Distributions were generated by 12 QDs tracking of microtubules targeting (n=2304 events), 11 QDs tracking of kinesin in cells (n=2328) and ten QDs tracking of kinesin *in vitro* (n=1130).

was calculated from the parabolic fitting on the MSD curves was 457 nm/s. This value is 10 times faster than velocity of microtubules, 50.3 nm/s.

MSD analysis describes the overall behavior of the molecules but does not provide detailed information about the movement. To investigate the detailed behavior of the dynamics of microtubules and kinesins, each trajectory in longitudinal (X direction) and transverse direction (Y direction) of microtubule was analyzed. Fig. 4 shows an example of the trajectory analysis for microtubules and kinesin molecules. The first column (Figs. 4A1, B1 and C1) shows the plots of the x and y positions versus time. The plus value of the x position means movement away from the nucleus or towards the plus end of the microtubule. While there is a large change in the position of x, the change of y position is relatively small in both the microtubule and the kinesin, indicating the movement is linear. However the direction of movement of the microtubules was changed more often than that of the kinesin.

The velocity averaged for the period of 0.5 s revealed a characteristic movement of kinesin in living cells (Figs. 4A2, B2, C2). As shown in Fig. 4B2, kinesin came to an almost stop ($V_x < 100$ nm/s), paused for a few seconds and then moved once again. This pause in the movement was observed in all the kinesin traces in 20 kinesin–QD conjugates in 5 cells. To compare the velocity of kinesin in cells with that in the *in vitro* assay, the kinesin–QDs were interacted with microtubules fixed on a coverslip and the movement of kinesin was observed under a total reflection fluorescence microscope [3]. Kinesin in the *in vitro* assay moved smoothly with an almost constant velocity (Fig. 4C) and they seldom stopped for more than a few seconds. The difference between the velocity of kinesin in cells and the *in vitro* is clearly demonstrated in the histograms of Figs. 4B3 and C3; high frequency at low velocity <100 nm/s in cells but low frequency in the *in vitro*. This result indicates that the "stop and go" behavior of kinesin is a unique phenomenon that occurs in the only cells but not in the *in vitro* assay. The "stop and go" behavior of kinesin is similar to previous reports of the vesicle transport by dynein in cultured cells and mice tumor cells [13,30]. Our data, however, is inconsistent with a previous report that the distributions of kinesin velocity in cells and *in vitro* are remarkably similar [21]. The difference could be due to the difference species of kinesin, mouse kinesin-1 in this study and drosophila kinesin-1 in the previous work. It could also be possible that movement of mouse kinesin is regulated by microtubule associated proteins such as tau which inhibits kinesin movement presumably by steric blocking [13,31,32].

Discrepancies were also found between the velocities of kinesin in cells and in the *in vitro* assay. The maximum velocity of kinesin in cells was 1.5–2.4 μm/s observed with the small portion in velocity of kinesin (Fig. 4B2). The maximum velocity of kinesin in the *in vitro* assay was up to 1.2 μm/s which is considerably slower than that in cells (Fig. 4C2). A simple explanation for this discrepancy is that the apparent velocity of kinesin in cells includes the velocity of the microtubules. Interestingly, the maximum speed that vesicles move in a living cell is often significantly higher than kinesin motors measured in *in vitro* systems [33,34]. Our results suggest that the fast movement of vesicles is related to the dynamics of both kinesin and microtubules. Identifying the unique behavior of the motor proteins in living cell is an important goal to understand intracellular traffics and cell division for future work.

Bio-conjugated QDs were successfully delivered into cells, and hundreds of single QDs were tracked for long periods of time. Our work also shows that the antibody and kinesin did not lose their function within living cells, suggesting that this new method is also applicable for investigation of other proteins. The major advantage of this method is that it is possible to track single QDs with bright fluorescence within living cells for long periods of time with high temporal and spatial resolution. The next step will be to observe the movement with higher precision, sub-milliseconds and 1 nm, within living cells to investigate natural function and molecular mechanism of the proteins [13,27,34]. Another approach will be to image several different of molecules within single cells at the same time. The general method described here is an excellent method for intracellular targeting proteins and for investigation of behavior of purified protein. This approach opens new avenues for studying living cells in biology and medical science.

Acknowledgments

We gratefully acknowledge J.M. West for critical reading of this manuscript. This work was supported by Grants-in-Aid for Scientific Research in Priority Areas from the Japan MEXT (H.H.), and Special Coordination Funds for Promoting Science and Technology of JST (H.H. and K.G.) and CREST of JST (H.H.).

Appendix A. Supplementary data

Supplementary data associated with this article can be found, in the online version, at doi:10.1016/j.yexcr.2008.09.014.

REFERENCES

[1] A. Ishijima, T. Yanagida, Single molecule nanobioscience, Trends Biochem. Sci. 26 (2001) 438–444.
[2] S. Toba, T.M. Watanabe, L. Yamaguchi-Okimoto, Y.Y. Toyoshima, H. Higuchi, Overlapping hand-over-hand mechanism of single molecular motility of cytoplasmic dynein, Proc. Natl. Acad. Sci. 103 (2006) 5741–5745.
[3] R.D. Vale, T. Funatsu, D.W. Pierce, L. Romberg, Y. Harada, T. Yanagida, Direct observation of single kinesin molecules moving along microtubules, Nature 380 (1996) 451–453.
[4] A. Yildiz, J.N. Forkey, S.A. McKinney, T. Ha, Y.E. Goldman, P.R. Selvin, Myosin V walks hand-over-hand: single fluorophore imaging with 1.5-nm localization, Science 300 (2003) 2061–2065.
[5] Y. Sako, T. Yanagida, Single-molecule visualization in cell biology, Nat. Rev. Mol. Cell Biol. Suppl (2003) SS1–SS5.
[6] X.S. Xie, J. Yu, W.Y. Yang, Living cells as test tubes, Science 312 (2006) 228–230.
[7] M. Bruchez Jr, M. Moronne, A.P. Alivisatos, Semiconductor nanocrystals as fluorescent biological Labels, Science 281 (1998) 2013.
[8] W.C.W. Chan, S. Nie, Quantum dot bioconjugates for ultrasensitive nonisotopic detection, Science 281 (1998) 2016–2018.
[9] J.K. Jaiswal, H. Mattoussi, J.M. Mauro, S.M. Simon, Long-term multiple color imaging of live cells using quantum dot bioconjugates, Nat. Biotechnol. 21 (2003) 47–51.
[10] S. Li-Shishido, T.M. Watanabe, H. Tada, H. Higuchi, N. Ohuchi, Reduction in nonfluorescence state of quantum dots on an

immunofluorescence staining, Biochem. Biophys. Res. Commun. 351 (2006) 7–13.
[11] X. Wu, H. Liu, J. Liu, K.N. Haley, J.A. Treadway, J.P. Larson, N. Ge, F. Peale, M.P. Bruchez, Immunofluorescent labeling of cancer marker Her2 and other cellular targets with semiconductor quantum dots, Nat. Biotechnol. 21 (2003) 41–46.
[12] D.S. Lidke, P. Nagy, R. Heintzmann, D.J. Arndt-Jovin, J.N. Post, H.E. Grecco, E.A. Jares-Erijman, T.M. Jovin, Quantum dot ligands provide new insights into erbB/HER receptor-mediated signal transduction, Nat. Biotechnol. 22 (2004) 198–203.
[13] T.M. Watanabe, H. Higuchi, Stepwise movements in vesicle transport of HER2 by motor proteins in living cells, Biophys. J. 92 (2007) 4109–4120.
[14] M. Dahan, S. Levi, C. Luccardini, P. Rostaing, B. Riveau, A. Triller, Diffusion dynamics of glycine receptors revealed by single-quantum dot tracking, Science 302 (2003) 442–445.
[15] I.L. Medintz, H.T. Uyeda, E.R. Goldman, H. Mattoussi, Quantum dot bioconjugates for imaging, labelling and sensing, Nat. Mater. 4 (2005) 435–446.
[16] K.-S. Huang, Y.-C. Lin, K.-C. Su, H.-Y. Chen, An electroporation microchip system for the transfection of zebrafish embryos using quantum dots and GFP genes for evaluation, Biomed. Microdevices 9 (2007) 761–768.
[17] A.M. Derfus, W.C.W. Chan, S.N. Bhatia, Intracellular delivery of quantum dots for live cell labeling and organelle tracking, Adv. Mater. 16 (2004) 961–966.
[18] E.B. Voura, J.K. Jaiswal, H. Mattoussi, S.M. Simon, Tracking metastatic tumor cell extravasation with quantum dot nanocrystals and fluorescence emission-scanning microscopy, Nat. Med. 10 (2004) 993–998.
[19] H. Duan, S. Nie, Cell-penetrating quantum dots based on multivalent and endosome-disrupting surface coatings, J. Am. Chem. Soc. 129 (2007) 3333–3338.
[20] A. Hoshino, K. Fujioka, T. Oku, S. Nakamura, M. Suga, Y. Yamaguchi, K. Suzuki, M. Yasuhara, K. Yamamoto, Quantum dots targeted to the assigned organelle in living cells, Microbiol. Immunol. 48 (2004) 985–994.
[21] S. Courty, C. Luccardini, Y. Bellaiche, G. Cappello, M. Dahan, Tracking individual kinesin motors in living cells using single quantum-dot imaging, Nano Lett. 6 (2006) 1491–1495.
[22] D. Kutz, M. Burg, Evolution of osmotic stress signaling via MAP kinase cascades, J. Exp. Biol. 201 (1998) 3015–3021.
[23] L. Wasungu, D. Hoekstra, Cationic lipids, lipoplexes and intracellular delivery of genes, J. Control. Release 116 (2006) 255–264.
[24] A. Kusumi, C. Nakada, K. Ritchie, K. Murase, K. Suzuki, H. Murakoshi, R.S. Kasai, J. Kondo, T. Fujiwara, Paradigm shift of the plasma membrane concept from the two-dimensional continuum fluid to the partitioned fluid: High-speed single-molecule tracking of membrane molecules, Annu. Rev. Biophy. Biomol. Struct. 34 (2005) 351–378.
[25] W.J. Parak, R. Boudreau, M.L. Gros, D. Gerion, D. Zanchet, C.M. Micheel, S.C. Williams, A.P. Alivisatos, C. Larabell, Cell motility and metastatic potential studies based on quantum dot imaging of phagokinetic tracks, Adv. Mater. 14 (2002) 882–885.
[26] J. Howard, Mechanics of Motor Proteins and the Cytoskeleton, Sinanuer Associates, 2001.
[27] X. Nan, P.A. Sims, P. Chen, X.S. Xie, Observation of individual microtubule motor steps in living cells with endocytosed quantum dots, J. Phys. Chem. B 109 (2005) 24220–24224.
[28] J. Howard, A.J. Hudspeth, R.D. Vale, Movement of microtubules by single kinesin molecules, Nature 342 (1989) 154–158.
[29] A. Yildiz, M. Tomishige, R.D. Vale, P.R. Selvin, Kinesin walks hand-over-hand, Science 303 (2004) 676–678.
[30] H. Tada, H. Higuchi, T.M. Wanatabe, N. Ohuchi, In vivo real-time tracking of single quantum dots conjugated with monoclonal anti-HER2 antibody in tumors of mice, Cancer Res. 67 (2007) 1138–1144.
[31] R. Dixit, J.L. Ross, Y.E. Goldman, E.L.F. Holzbaur, Differential regulation of dynein and kinesin motor proteins by tau, Science 319 (2008) 1086–1089.
[32] B. Trinczek, A. Ebneth, E.M. Mandelkow, E. Mandelkow, Tau regulates the attachment/detachment but not the speed of motors in microtubule-dependent transport of single vesicles and organelles, J. Cell. Sci. 112 (1999) 2355–2367.
[33] D.B. Hill, M.J. Plaza, K. Bonin, G. Holzwarth, Fast vesicle transport in PC12 neurites: velocities and forces, Eur. Biophys. J. 33 (2004) 623–632.
[34] C. Kural, H. Kim, S. Syed, G. Goshima, V.I. Gelfand, P.R. Selvin, Kinesin and dynein move a peroxisome in vivo: a tug-of-war or coordinated movement? Science 308 (2005) 1469–1472.

●特 集● がん分子イメージングの新展開

がん分子イメージングの新展開

武田 元博[*1] 権田 幸祐[*1] 樋口 秀男[*2] 大内 憲明[*3]

〔*Jpn J Cancer Chemother* 35(8): 1277-1280, *August*, 2008〕

In Vivo Single Molecular Fluorescence Imaging for Analysis of Pharmacokinetics: Motohiro Takeda[*1], Kohsuke Gonda[*1], Hideo Higuchi[*2] and Noriaki Ohuchi[*3] ([*1]*Division of Nano-Medical Science, Graduate School of Medicine, Tohoku University*, [*2]*Dept. of Physics, Graduate School of Science, The University of Tokyo*, [*3]*Division of Surgical Oncology, Graduate School of Medicine, Tohoku University*)

Summary

Nano-materials are expected for research on molecular imaging of pharmacokinetics. We measured *in vivo* migration of CdSe nano-particles (Quantum Dots (QDs)) conjugated with monoclonal anti-HER2 antibody (trastuzumab) in tumor vessel to breast cancer cells. We established a high resolution *in vivo* 3D microscopic system for a novel imaging method at single molecular level. The HER2 protein expressed in cancer cells and its dynamics were visualized by QDs *in vivo* at the spatial resolution of 30 nm. It suggests future utilization of the system in medical applications to improve the drug delivery system to target primary and metastatic tumors for made-to-order treatment. Future innovation in cancer imaging by nano-technology and novel measurement technology will provide great improvement, not only in the clinical field, but also in basic medical science. Advances in nano-biotechnology have great potential to improve prevention, diagnosis and treatment of human disease. **Key words**: Molecular imaging, Fluorescence, **Corresponding author**: Motohiro Takeda, Division of Nano-Medical Science, Graduate School of Medicine, Tohoku University, 1-1 Seiryo-machi, Aoba-ku, Sendai 980-8574, Japan

要旨 現在様々な機能をもつナノ粒子が作製されつつあり，その多くは医療応用が期待されている。われわれはナノ粒子を利用した分子イメージングに取り組み，蛍光ナノ粒子に抗体治療薬を結合させることにより抗体治療薬であるtrastuzumabの体内動態を検出することに成功した。従来1分子レベルで *in vivo* 計測できた例はなく，高感度な計測システムを併用することでこれまでにない，薬物のDDSを計測する手法が確立されつつある。今後，この手法により新たなDDSが開発されることが期待される。

はじめに

がんは1985年以降，日本人の死因の第1位を占めており，働き盛りの年代のがん死は人口の急速な高齢化が進むわが国において，最も緊急に改善しなければならない課題の一つである。そのためにはがんの早期診断と適切な治療が重要であり，画像診断・イメージングが非常に大きな役割を担っている。従来のX線画像診断に加え，近年の生体物質の計測技術の進歩により，これまでは計測できなかった分子の分布が計測可能になりつつある。以下に分子の分布を計測する手法を列挙する。プロトン分布から水の分布を計測する手法がMRIとして用いられ，また水の拡散定数を計測できることから，がんの診断に応用する試みが行われている。positron emission tomography (PET) では，炭素や窒素原子をラベルすることで組織血流量，種々の基質代謝量，酵素反応，受容体結合能など細胞の機能をイメージングすることが可能である。がん腫による相違があるものの，高い糖代謝を利用して描出するFDG-PETが，がん診断に広く利用されている。最近はmagnetic resonance spectroscopy (MRS) で各元素独自の信号を検出することにより生体内の様々な元素の解析，イメージングも行われつつあ

[*2] 東京大学理学部・物理学科
[*3] 東北大学大学院医学系研究科・腫瘍外科学分野

連絡先: 〒980-8574 仙台市青葉区星陵町1-1 [*1] 東北大学大学院医学系研究科・ナノ医科学寄附講座
武田 元博

0385-0684/08/¥500/論文/JCLS

る。これらはマーカーとなる分子が一定量以上存在することで検出可能となる。

その一方で生体分子に対する様々な抗体が作製され，これら抗体と蛍光マーカーなどを結合させて生体分子マーカーとし，受容体蛋白などを標的とした生体蛋白や薬物の動態を1分子レベルで計測する技術が出現し，drug delivery system（DDS）の評価や開発に利用しようとする動きがみられる。このような技術には高感度な検出を可能とするマーカーの存在および高精度な検出技術が必須である。ここで，高感度検出が可能なマーカーの有力な候補として，様々なナノ粒子をあげることができる。ナノテクノロジーは従来にない機能をもった物質を生みだしつつあり，ナノ粒子の多くは医療においても利用可能であると考えられ，現在様々な応用が試みはじめられている。われわれは，がん診療において，診断から治療に至るまでの様々な診療段階で機能性ナノ粒子を医療応用することをめざして研究を行ってきた。

本稿では医療において求められるナノテクノロジーへの期待とわれわれの取り組みを中心として，Ⅰ．医療における分子イメージング，Ⅱ．機能性ナノ粒子の種類，Ⅲ．われわれが開発している新しい機能性ナノ粒子と1分子イメージングへの応用，Ⅳ．機能性ナノ粒子を用いたイメージングの今後の展開について解説する。

Ⅰ．医療における分子イメージング

分子イメージングとは，分子の存在や動きを可視化することであり，多数の分子の集まりをマクロレベルで検出する技術や1分子の存在を検出する技術がこれに含まれる。特定の分子を検出する方法として，ある分子にマーカーをラベルし，そのマーカーが発するシグナルを検出する方法と，その分子自身が発するシグナルを検出する方法とがある。分子マーカーとして放射性同位元素，蛍光色素，磁性ビーズ，色素などがあげられる。放射性同位元素としては^{99m}Tcや^{201}Tl，^{67}Ga，^{125}Iなど従来用いられてきたガンマ線を放出する核種や，^{11}C，^{18}F，^{13}N，^{15}Oなど，陽電子を発生し体内の電子と結合して消滅する際，対向する2方向にガンマ線を発する核種などがすでにシンチグラフィーやSPECT（single photon emission tomography），PET（positron emission tomography）で幅広く用いられている。分子そのものの発するシグナルを検出する方法としてMRIがあげられる。1分子レベルで分子の検出を行う場合，目的とする分子1個をそのまま検出できるとは限らず，むしろそのような分子はまれであることから，多くの場合1分子レベルの検出にはその分子を他の検出可能なマーカーでラベルして検出する方法が用いられる。

医療における基本的な三つの柱は疾患の予防，診断，治療であり，特にがん診療において病巣特定のためのイメージングは重要である。悪性疾患の治療を行う前には正確な診断が必要であり，最初に組織診による病名診断，次いで病期を明らかにしなければならない。病期診断において，非常に重要な役割を担っているのが画像診断であり，特に造影剤を用いた画像診断は固形がんの部位診断に欠かせない。X線CTやMRI，PETなどの新しい画像診断は従来の単純X線写真に頼った診断法を一変させた。すなわち従来得ることのできなかった三次元情報が得られるようになったのである。正確な病巣の拡がり診断により臓器を全切除することなく，温存する手術が容易に行えるようになった。さらに，がんの代謝機能を検出するPETの出現で質的診断を可能とする画像診断も出現した。FDG-PETは，がんの活発な糖代謝を利用してマーカーを集積させる機能的診断といえる。このように様々な画像診断法は，造影剤や機能的マーカーによって病巣を可視化することで診断から外科治療・放射線治療などの局所療法を行う際，治療範囲の決定や，化学療法の効果判定のための重要な手段となっている。

以上のように分子イメージングは，従来の生体の形態のみでなく，生体機能を直接計測するための手法として徐々にその領域を拡げつつある。

Ⅱ．機能性ナノ粒子

近年，従来にはみられない機能，構造をもつナノ粒子が数多く開発されつつある。ナノ材料の作製法は大別して，分子レベルでナノ材料を合成するボトムアップ法と，従来存在する物質を分解・分割してより小さな物質を作るトップダウン法の二つの異なる物質制御技術からなる。現在ではin-silico designと呼ばれる，スーパーコンピュータを用いたシミュレーションによって有用かつ安定な化学構造を予測し合成する手法や，逆に合成した物質の物性からシミュレーションによって構造を予測する手法が出現するなど，単に化学のみではなくコンピュータサイエンスなど多くの工学分野がナノテクノロジーの発展に関与している。このようにナノレベルの物質制御技術は現在急速な勢いで発展し，そこから生みだされた様々な物質は，われわれの生活のみならず医療技術を大きく変える可能性を秘めている。たとえば，ナノサイズへ微小化された電子回路の部品やこれらを組み合わせてできたデバイスによるマイクロまたはナノサイズの装置や，新たな機能を付与して創製された分子・クラスターなどの物質があげられ，これらの技術は従来の化学合成を中心とした“もの作り”をベースとして，分子構造のシミュレーションやナノメートルオーダーの計測技術な

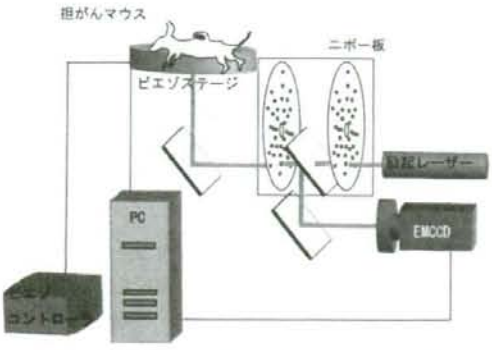

図1 *In vivo* 単分子蛍光計測システムの模式図

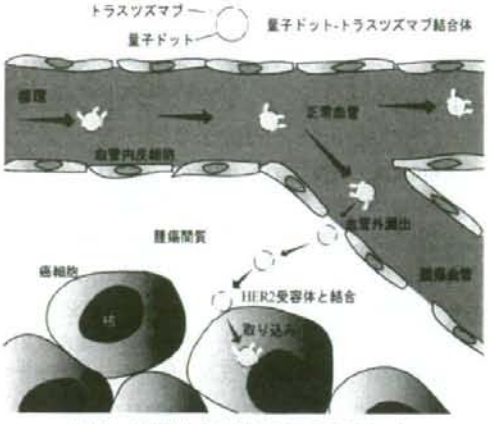

図2 血管内から細胞内に至る量子ドット—trastuzumab 結合体の体内動態

と，新しい技術を巻き込みながらさらに発展していこうとしている。

医療応用可能なナノ粒子として，量子ドット，金コロイド，ヨウ化銀ビーズなどの無機物から，デンドリマー[1]，リポソーム[2]，高分子ミセル[3]およびウイルスの外套蛋白のクラスターを利用した中空ナノ粒子などの有機物まで，極めて多彩なナノ材料がこれまでに作製されてきた。ナノ粒子は数百ナノメートル以下の大きさをもつ粒子と定義され，表面に付着した機能分子による機能付与ばかりでなく，後述するように大きさそのものが機能をもつ場合がある。人工的に作られたナノ粒子は，それぞれ様々な目的で作られており，たとえば量子ドットは優れた蛍光特性をもち，有機系蛍光色素の20～30倍もの蛍光強度，高い耐光性，励起波長の多様性などを示す。ヨウ化銀ビーズはX線造影効果をもつ材料として作製されている。またデンドリマー[1]やリポソーム[2]，高分子ミセルなどは薬剤を内包する空間をもつことからdrug delivery system (DDS)に利用される[3]。DDSとは，薬剤を目的とする標的臓器・部位へ輸送するシステムのことであり，たとえばデンドリマーは樹枝状に伸びたポリマーの多数の枝の間に物質を挟み込み，またリポソームや高分子ミセルなどは中空であるため，内部に薬剤を内包することによってDDSに利用される。薬剤を内包することによって，薬剤が病巣に到達するまで健常部位に対する副作用を軽減し，病巣で薬剤を放出することによって病巣での効果的薬物濃度上昇を狙うのである。

機能性ナノ粒子を生体に投与する場合，病変部に特異的に集積してそれぞれの機能を発揮することはもちろん重要であるが，病変部以外に存在するナノ粒子の振る舞い，すなわち体内動態もナノ粒子の安全性に直結するため重要である。理想的には体内に蓄積することなく排泄または分解される必要があり，ナノ粒子は体内動態や排泄経路を考慮して作製されるべきである。

前述したように，ナノ粒子を医療応用する際，粒子サイズが大きな意義をもつ場合がある。それは悪性腫瘍の診断，治療におけるDDSとして利用する場合，特に有用である。悪性腫瘍が増殖するためには血流が欠かせないが，多くの悪性腫瘍は血管成長因子を直接分泌して自らの血管網を新生，構築する。腫瘍血管は急速に成長する腫瘍に対して血流を賄うため急速に構築される。そのためか通常の血管内皮と構造が異なり血管孔が大きいことが指摘されている[4]。その結果，正常血管内皮では通過し得ない数十～100 nmの物質を透過させることが知られている。この性質を利用して，100 nm程度またはそれ以下のナノ粒子を用い，腫瘍間質に選択的に取り込ませることで腫瘍への効率的なDDSを得ることができる（extended permeability and retention: EPR効果）。また，腫瘍選択的な薬剤の到達によって健常組織のダメージを軽減できると期待される。

Ⅲ．機能性ナノ粒子による1分子イメージングとDDS

1分子の動態を観察するためには分子マーカーを1個または少数レベルで検出する必要がある。現在，粒子1個レベルで検出し得る方法は蛍光計測法のみである。われわれは独自に開発した装置と，量子ドットを用いて生体内1粒子レベルの薬物動態の計測を試みてきた。生体内の1分子の動きを追跡するには高輝度な蛍光マーカーと高感度な蛍光計測装置，および計測時の生体の固定に工夫が必要である。

われわれが用いている装置は倒立顕微鏡，ニポー板式共焦点ユニット，高感度CCDカメラおよび励起用レーザーなどからなるイメージングシステム（図1）であり，HER2蛋白発現乳がんの治療に用いられる，モノクロー

ナル抗体治療薬である trastuzumab に量子ドットを結合させ（QT コンプレックス），HER2 蛋白発現乳がん細胞を移植したヌードマウスに静脈注射してその体内動態を 1 分子レベルで追跡することを試みた[5]。計測に当たって呼吸や心拍などの振動の影響を取り除くため，腫瘍表面の皮膚を切開し血管のつながった状態でガラス盤上に乗せ観察する手法（dorsal skin fold chamber）をとった。この手法により，1 分子の動きを空間分解能 30 nm，時間分解能 33 ms でとらえることに成功した。血管内から腫瘍間質に移送し，さらに細胞内に取り込まれた QT コンプレックスの移動をとらえた軌跡の模式図を図 2 に示す。QT コンプレックスは細胞内において停滞と直線運動を繰り返し，細胞膜付近の細胞質を移動した後，急激に核周囲に向かい，核付近で停滞する様子をとらえることができた。これまで trastuzumab は核内の cdk2 活性を抑制することが示唆されてきたが，今後この手法を応用することにより *in vivo* で証明することが可能と思われる。この手法は量子ドットが結合することで動態が修飾される懸念はあるものの，多くの抗がん剤の DDS を 1 分子レベルで直接確認する唯一の手法として利用価値がある。

Ⅳ．1 分子イメージング技術の将来への展望

以上のように生体 1 分子イメージングは臨床の場というよりはむしろ基礎レベルでの薬物動態や生体内での様々な機能を計測する際に有用と考えられる。従来分子の動態を直接観察する手段はなく，直接観察する手法が確立されることは，類推が関与する余地のない証明法として今後強力なツールとして活用されることが期待される。それはがん治療において，抗がん剤の動態のみならず，薬剤耐性のメカニズム解明やその解決，生体内での様々な分子動態，メカニズムをも解明する手法となることが期待される。

計測に用いる装置の特殊性や測定する生体の条件設定の難しさを差し引いても今後様々な領域での応用が期待される。

文　献

1) Tomalia DA, Baker H, Dewald J, *et al*: New class of polymers: starburst-dendritic macromolecules. *Polymer J* (Tokyo) **17**: 117-132, 1985.
2) Iga K, Ohkouchi K, Ogawa Y, *et al*: Membrane modification by negatively charged stearyl-polyoxyethylene derivatives for thermosensitive liposomes: reduced liposomal aggregation and avoidance of reticuloendothelial system uptake. *Drug Target* **2**(3): 259-267, 1994.
3) Nishiyama N, Okazaki S, Cabral H, *et al*: Novel cisplatin-incorporated polymeric micelles can eradicate solid tumors in mice. *Cancer Res* **63**(24): 8977-8983, 2003.
4) Maeda H and Matsumura Y: Tumoritropic and lymphotropic principles of macromolecular drugs. Critical reviews in therapeutic. *Drug Carrier Systems* **6**: 193-210, 1989.
5) Tada H, Higuchi H, Watanabe TM, *et al*: In vivo real-time tracking of single quantum dots conjugated with monoclonal anti-HER2 antibody in tumors of mice. *Cancer Res* **67**: 1138-1144, 2007.

新規開発ナノサイズヨウ化銀ビーズを用いたX線CT造影効果および体内動態の検討

武田 元博[1),2)]・桜井 遊[1)]・叢 莉蔓[1)]・小林 芳男[3)]・菅原 旭浩[4)]・大内 憲明[1)]

[1)] 東北大学腫瘍外科 [2)] 東北大学工学研究科 [3)] 茨城大学工学部 [4)] 東北大学放射線腫瘍学

1. はじめに

ナノレベルの物質制御技術は、現在急速な勢いで発展し、従来ない機能を持った物質を生み出しつつある。その中には医療に応用可能なものもあり、腫瘍や特定の臓器に集積する特性を生かした造影イメージングやドラッグデリバリーについて、種々の報告がなされてきた。しかし、ナノ粒子を実際に医療応用するためには生体に対するナノ粒子の安全性を確認することが最重要であるにもかかわらず、これらを実証した報告はこれまでほとんどなく、ナノ粒子の体内動態や排泄については未だ詳細な検討がなされていない現状にある。

一方で、現在の医療現場によく普及し、かつ有用なX線CTは、特に癌診療における腫瘍局在診断には欠かせない画像検査であり、とりわけ造影CTの重要性は高い。従来の造影剤は造影効果持続時間が数分と短いことが特徴であり、通常のCT撮影はこの特性に合わせ、殊に近年の高速CT撮影機種ではより短時間で撮影される。しかしそのため、例えば治療前後で病巣の遺残などを確認する際はCT撮影の度に何度も造影剤を投与しなければならない。また、外科手術においては、術後のQOLに大きな影響を与えるリンパ節郭清を省略するために、センチネルリンパ節生検が浸透し広く行われつつあるが、現在用いられているトレーサーにはそれぞれ欠点があり、これらの改善が求められている。つまり、センチネルリンパ節を同定するトレーサーとして、現在は色素やRIが一般的に用いられているが、色素法は安価かつ簡便であるものの手技習得に時間を要し、体外検出できないため単独での使用は推奨されず、また、RI法は体外検出が可能であり検出感度に優れるが、法的規制により使用できる施設に制限がある。これらの臨床上の要望に応えるべく、我々は新規ナノサイズヨウ化銀ビーズによる造影剤開発を試み、このX線造影剤によるセンチネルリンパ節の同定を着想した。X線CTはがん手術を行う施設の大多数にあり、しかも体外診断が可能という大きな特徴を有する。しかし従来の水溶性X線造影剤は投与後早期にリンパ節から流出するため、手術時にCT撮影でリンパ節を同定することは困難であった。ナノ粒子の多くは目的に応じたサイズ調整が可能であるため、適切な粒径を選択することで、リンパ節への長時間にわたる停滞が期待できると考えた。

今回我々はX線造影剤として新規に開発したナノサイズヨウ化銀ビーズを用い、ラットをモデルとして腫瘍における造影効果と持続時間、安全性について検討を行い、X線造影剤およびセンチネルリンパ節造影剤としてのヨウ化銀ビーズの医療応用を考える上で非常に重要な基礎的知見を得た。

2. ナノサイズヨウ化銀ビーズによる腫瘍のX線CT造影効果

腫瘍はヌードラット（F344/NJcl-*rnu*/*rnu*、オス、生後8－10週）背部皮下にラット腹水肝

連絡先：武田元博
〒980-8574 仙台市青葉区星陵町1-1
Tel: 022-717-7214 Fax: 022-717-7217
E-mail: motot@d1.dion.ne.jp

がん細胞株であるAH109A（東北大学医用細胞資源センターより供給）を1.0×10^{7}個皮下注射し、直径が約3cmになったものを用いた。ラット尾静脈内へ、我々が開発したナノサイズヨウ化銀ビーズ懸濁液（直径約30－70nm、2% w/vol懸濁液1mℓ/kg、図1）[1]を投与し、投与前、および10、30、60分後にそれぞれCT画像を撮影した。CTは東芝メディカルシステム株式会社製Asteionを使用した。スライス厚は3㎜である。CT値の解析にはAZE社のVIRTUAl PLACE LIVERTY®を用いた。

腫瘍は、造影1時間後まで、時間経過に伴い、緩徐かつ有意なCT値の増強を認めた（図2）。

近年、ナノ粒子はEPR (extended permeability and retention) 効果によって腫瘍に受動的に蓄積することが報告されている[2]。その理由として腫瘍血管の透過性亢進が指摘されており、この性質を利用し腫瘍に集積しやすい適切なサイズを明らかにすることで、より効果的ながん治療、および有用なドラッグデリバリーシステムとしての応用が可能と考えられ、現在更なる検討を進めている。ナノ粒子造影剤は造影時間が持続する特徴を有するため、外科手術において切除範囲を手術前後に確認する際、非常に有用と考えられる。更にCTを備える手術場では、術前の一回の造影剤投与のみで術中の病巣確認も可能と考えられ、臨床応用が期待される。

3. ナノサイズヨウ化銀ビーズによる膝窩リンパ節のX線CT造影効果

ラットはドンリュウ（オス、生後8－10週）を用いた。ナノサイズヨウ化銀ビーズ懸濁液（直径約30－70nm、2% w/vol懸濁液1mℓ/kg）0.2mℓをラット足背皮下に注射し、投与前、および15、30、60分後に膝窩のCT撮影を行った。CTは東芝メディカルシステム株式会社製Asteionを使用した。スライス厚は2㎜である。CT値の解析にはAZE社のVIRTUAl PLACE LIVERTY®を用いた。

ヨウ化銀ビーズのCT値は投与前に比較し、緩徐かつ有意な増加を示した（図3）。冒頭にも述べたように侵襲的なリンパ節郭清を省略で

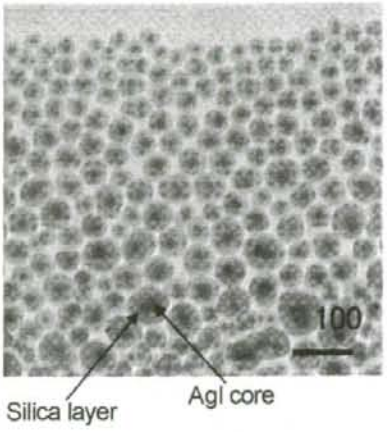

図1 ヨウ化銀ビーズの透過型電子顕微鏡像
ヨウ化銀ビーズは、ヨウ化銀を中心核とし、周囲をシリカでコーティングされた2層構造を有する。

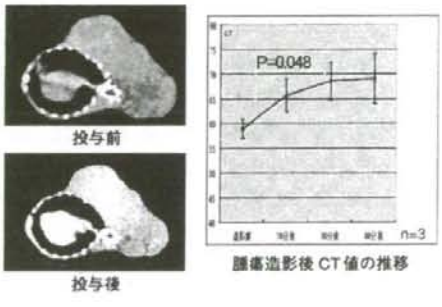

図2 ラット腫瘍のナノサイズヨウ化銀ビーズによる造影X線CT像とCT値の変化

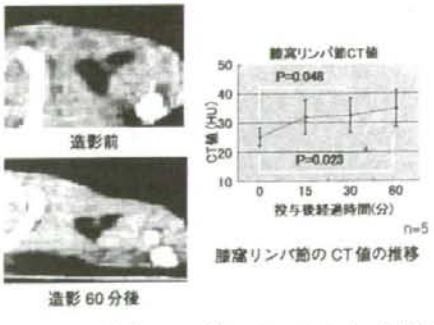

図3 ラット膝窩リンパ節のナノサイズヨウ化銀ビーズによる造影像とCT値の変化

きるセンチネルリンパ節生検法は今後、がん診療においてテイラーメイド治療を推進する上で重要な役割を果たすと考えられる。この際リンパ節を比較的長い時間造影できることの意義は大きく、術中のリンパ節の位置や郭清範囲の同定に有効な手段となりうる。

4. 安全性の評価

ナノ粒子の安全性に関しては、ナノテクノロジーの発展に伴い世界各国で大規模なプロジェクトが立ち上げられ検討されているが[3,4]、その投与法（皮膚・皮下・静脈・経口投与、吸入など）により、安全域は異なる。

我々の作製したナノサイズヨウ化銀ビーズのLD50は、Litchfield-Wilcoxon法により1.26mℓ(74.2mg)/kgと算出され、至適投与量を58.6mg/kgと設定した。今回行ったヨウ化銀ビーズの安全性評価によって、投与量と同時にビーズ懸濁液の分散性は非常に重要な要因であることが明らかになった。当初、ヨウ化銀ビーズ懸濁液70.42mg/kg以上の投与では、ほぼ過半数の死亡例を認め、死亡例のほとんどで投与直後の呼吸停止を認めた。原因として、ヨウ化銀ビーズが粒子間で凝集を起こしやすい傾向を有するため、塞栓症を起こした可能性が考えられた。そのため、投与直前に超音波による分散を15分間施行した後、緩徐に投与するなどの改善策を講じたところ、至適投与量58.6mg/kgでの死亡例は10%以下に減少し、組織の顕微鏡観察でも血栓の形成は認められなかった。

ナノ粒子の臓器分布を電子顕微鏡で観察することは排泄経路を検討する上で有用である。今回特に造影効果の高い脾臓と肝臓について透過型電子顕微鏡を用いて観察を行った。その結果、脾臓では静脈洞のみにナノサイズヨウ化銀ビーズが集積し、肝臓では肝細胞にナノサイズヨウ化銀ビーズが取り込まれている様子が観察された（図4）。現在、誘導結合プラズマ法による組織内の銀の定量分析を行い、詳細な分布、排泄経路について検討を進めている。

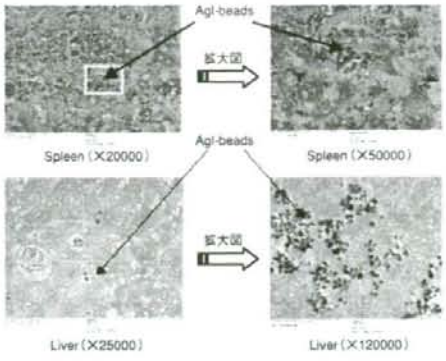

図4 ナノサイズヨウ化銀ビーズ投与ラットの脾および肝の透過型電子顕微鏡像

5. おわりに

新規開発したヨウ化銀ビーズについて、CTおよび透過型電子顕微鏡を用いて、造影効果や体内分布について検討を行った結果、ナノサイズヨウ化銀ビーズは従来の造影剤に比べ長時間の造影効果を維持することがわかった。一定の粒径を持つナノ粒子を用いることで、従来なし得なかった、一定時間以上持続するX線CT造影剤の開発が可能である。また、ヨウ化銀ビーズはシリカコーティングで形成されるその特徴的な2層構造により電子顕微鏡で観察可能であることが今回示されたが、現在一般に使用されているナノ粒子はこのような特徴を有しないため、臓器を電子顕微鏡で観察した際、生体内のタンパク物質と区別することが難しい。バイオマーカーとしての応用を考えた際、電子顕微鏡による直接観察は非常に大きなメリットであり、今回の結果から、多重構造を持つナノ粒子を用いることにより、投与したナノ粒子の体内動態を電子顕微鏡で直接検証可能であることが示唆された。

ナノ粒子の様々な特徴を生かした研究は世界規模で行われており、ナノテクノロジーに対する期待は大きい。特に表面のコーティングは体内動態をコントロールする上で極めて重要と考えられており[5]、シリカコーティングの体内動態、安全性の検討を更に進めなければならない。今後様々なナノ粒子を臨床に応用するためには

慎重な検討を積み重ねる必要があるものの、ナノテクノロジーにはこれからの医療を大きく変える可能性が秘められており、今後の精力的な研究の展開が期待される。

参考文献

[1] Kobayashi, Y. et al: Silica-coating of AgI semiconductor nanoparticles, Colloids and Surfaces A: Physicochemical and Engineering Aspects 251: 197-201, 2004

[2] Li, J. et al: In vitro study of drug accumulation in cancer cells via specific association with CdS nanoparticles, Bioorganic & Medicinal Chemistry Letters 16: 4808-4812, 2006

[3] Thomas, K. et al: Research strategies for saftety evaluation of nanomaterials, part Ⅰ: evaluating the human health implications of exposure to nanoscale materials, Toxicol Sci 87: 316-321, 2005

[4] Thomas, K. et al: Research strategies for safety evaluation of nanomaterials, part Ⅷ: International efforts to develop risk-based safety evaluations for nanomaterials, Toxicol Sci 92: 23-32, 2006

[5] Lockman, PR. et al: Nanoparticle surface charges alter blood-brain barrier integrity and permeability, J Drug Target 12: 635-641, 2004

Microelectronics Journal 40 (2009) 218–220

Contents lists available at ScienceDirect

Microelectronics Journal

journal homepage: www.elsevier.com/locate/mejo

ZnO clusters: Laser ablation production and time-of-flight mass spectroscopic study

A. Dmytruk [a,d,*], I. Dmitruk [b,d], I. Blonskyy [a], R. Belosludov [c], Y. Kawazoe [c], A. Kasuya [d]

[a] Institute of Physics of National Academy of Sciences of Ukraine, Kyiv 03028, Ukraine
[b] Physics Department, National Taras Shevchenko University of Kyiv, Kyiv 03122, Ukraine
[c] Institute for Materials Research, Tohoku University, Sendai 980-8577, Japan
[d] Center for Interdisciplinary Research, Tohoku University, Sendai 980-8578, Japan

ARTICLE INFO

Available online 9 September 2008

Keywords:
Zinc oxide
Cluster
Magic number
Time-of-flight mass spectroscopy

ABSTRACT

Zinc oxide clusters have been produced by laser ablation of bulk powder zinc peroxide in vacuum and investigated by time-of-flight mass spectroscopy. Experimental results revealed unpredicted and hitherto unknown $(ZnO)_n$ clusters of enhanced stability ("magic clusters") at $n = 34$, 60 and 78. Cage-like structures for the magic clusters have been suggested, supported by first-principles calculations.

1. Introduction

Decrease of the size of functional elements is the mainstream of microelectronics industry evolution. Reaching the nanometer scale, however, the properties of objects are determined not only by their composition, but also by their size, shape and structure. Drastic changes of material properties appear in transition region between solid state and atoms (molecules), i.e. in the range below about 200 monomers (constituting elements). Clusters of this range have a practical value only if they possess an enhanced stability ("magic clusters"), like the well-known carbon fullerenes [1], or the recently discovered CdSe magic particles [2]. The other advantage of magic clusters is the atomic precision of their composition that considerably simplifies experimental research on nanomaterials and much spreads their applications, especially when a regular arrangement of nanostructures is necessary. Among others, ZnO is of interest as a promising material for photovoltaics, optoelectronics, spintronics, photoelectrochemistry and others, and deserves special attention for biomedical applications, as it is low toxic. The exciton Bohr radius of ZnO is about 1.8 nm, meaning that strong quantum confinement effects could be observed for clusters consisting of less than a 1000 of ZnO monomers, approximately, if we consider cluster's density the same as for bulk material that emphasizes the interest to the small $(ZnO)_n$ clusters.

A possibility for ZnO to form spheroids (fullerenes) has been predicted theoretically, suggesting $n = 12$ and 16 as the magic numbers [3], and stable three-dimensional spheroid structures for $n = 8$, 9 and larger [4]. Zn_2O_2 and Zn_3O_3 rings have been suggested as building blocks for larger spheroid clusters. Recent studies [5] extended the range of calculated ZnO clusters up to $n = 64$; however, not all the clusters in the range have been studied, but $n = 9$–16, 18, 20, 22, 24, 28, 36, 48 and 64 only. It has been shown that "bubble-like" cluster structure is energetically more favorable than the wurtzite structure for $n < 26$, while the wurtzite structure is more stable for $n \geq 26$ and larger clusters. Also, the "onion-like" cluster $(ZnO)_{60}$, constructed by putting $(ZnO)_{12}$ cage inside of $(ZnO)_{48}$ cage, has been shown to be more stable than $(ZnO)_{64}$ bubble-like cluster by about 0.2 eV/atom. Very recently, it has been reported that the onion-like and bulk-like isomers are progressively more stable with increasing size, but cage and tube structures are the most preferred structural motifs for $(ZnO)_n$ with $n = 24$, 28, 36 and 48 [6]. Thus, the extensive calculations done still do not cover the whole range of small ZnO clusters, and their results partially contradict each other.

A large number of extensive experimental studies were done on zinc oxide (ZnO) nanoparticles of several nanometers and larger scale, containing hundreds and much more of ZnO monomers. However, only a few papers deal with small $(ZnO)_n$ clusters, and they all are limited to $n < 20$ only. Typically, the clusters were produced by laser ablation of ZnO powder in vacuum, and no magic numbers were found in mass spectra [7,8]. Recent studies on synthesized by electroporation of vesicles, uncapped small $(ZnO)_n$ clusters showed oscillating red and blue shifts of the characteristic absorption band from $n = 1$ to 15, while no peculiarities were observed for $n > 15$ [9]. Overall, both experimental and theoretical studies of $(ZnO)_n$ clusters of $n > 20$ with the atomic precision are scarce.

Here, we present time-of-flight (TOF) mass spectroscopic studies on ZnO clusters of up to about a hundred of monomers,

* Corresponding author at: Institute of Physics of National Academy of Sciences of Ukraine, Kyiv 03028, Ukraine. Fax: +380 44 525 1543.
E-mail address: admytruk@gmail.com (A. Dmytruk).

0026-2692/$ - see front matter © 2008 Elsevier Ltd. All rights reserved.
doi:10.1016/j.mejo.2008.07.010

and propose possible structures for the extra stable clusters, supported by extensive first-principles calculations.

2. Experimental

ZnO clusters were formed by laser ablation of bulk powder zinc peroxide (ZnO_2) in a Bruker Reflex III-T TOF mass spectrometer. ZnO_2 powder (WAKO) was mixed with a small amount of solvent (distilled water or toluene), and with alkylamine matrix (decylamine or dodecylamine, WAKO) in some experiments. About 1 μl of the resulting suspension was dropped on a stainless steel target, dried in vacuum, and the target was inserted in the mass spectrometer. The spectrometer was equipped with a nitrogen laser, which produced 4 ns pulses of 337.1 nm wavelength light with 300 μJ energy at 1–3 Hz repetition rate. The laser beam was passed though a controlled attenuator (typically about 10% attenuation level was used) and focused into about 20 μm spot on the target. Cooling by carrier gas injection was not used. Produced ions were accelerated by a potential of 19 kV, separated in the flight tube either in linear or in reflex mode, and registered by a microchannel plate detector. Positively or negatively charged clusters were measured, depending on the polarity of the accelerating potential. Typically the reflex mode was used, and the spectrum was acquired by accumulating the signal of about 500 laser shots.

3. Results and discussion

ZnO_2 has essentially different properties from ZnO, namely a much lower thermolysis temperature (150 °C for ZnO_2 and 1975 °C for ZnO) and density (1570 and 5600 kg/m^3, respectively). The differences indicate much weaker interatomic bonds in ZnO_2 than in ZnO. Practically, that makes ZnO_2 powder a much more efficient precursor for ZnO clusters than the ZnO powder used in previous laser ablation experiments [7,8]. The excess oxygen in ZnO_2 may volatilize during laser ablation. Therefore, using of ZnO_2 is a crucial factor for efficient production of ZnO clusters by laser ablation.

Fig. 1 shows a TOF mass spectrum of positively charged clusters obtained by laser ablation of ZnO_2 powder. The spectrum consists of a series of peaks separated by about 81.42 amu, which corresponds to the mass of ZnO (81.39 amu). The complete series of $(ZnO)_n$ clusters can be reliably resolved up to more than a hundred of ZnO monomers. $(ZnO)_{34}$, $(ZnO)_{60}$, and $(ZnO)_{78}$ clusters are significantly more abundant than their neighbors in the series, that allows to call them "magic clusters". $(ZnO)_{60}$ is the most remarkable among them. Although it is difficult to compare quantitatively the occurrence of magic and non-magic clusters produced and studied in this experiment, the observed small advantage of the magic clusters could result in significant dominance of these clusters being produced by some other methods. For example, TOF mass spectra of carbon clusters obtained by laser ablation of graphite [10] and other carbon compounds [11] show just slightly higher occurrences of C_{60} clusters than of the others, while optimization of cluster formation conditions allowed much more effective C_{60} production [1].

The reported results of calculations on ZnO clusters are scarce for the observed magic numbers, therefore applicable models of other binary compounds should be considered to suggest the structures for ZnO. The closest allies are other II–VI and III–V group compounds. Among them, CdSe and BN clusters are the best studied.

As ZnO belongs to II–VI group, it is no wonder to find in ZnO series the magic cluster of 34 monomers which found commonly for other group members (ZnS, ZnSe, ZnTe, CdS, CdSe, CdTe) [10], and to suppose its structure is the same as the structure of the well-studied $(CdSe)_{34}$ [2].

The magic cluster of 60 monomers was not experimentally observed hitherto either for II–IV or for III–V group compounds. However, some theoretical studies have been performed: an onion-like structure has been calculated recently for $(ZnO)_{60}$ [5], whilst the empty cage has been suggested earlier for $(BN)_{60}$ [12]. Our ongoing extensive first-principles calculations nominate the $(ZnO)_{12}$ @ $(ZnO)_{48}$ nested cage as the most stable isomer of $(ZnO)_{60}$.

The structure of $(ZnO)_{78}$ magic cluster is not clear yet. Presumably, it consists of six $(ZnO)_{12}$ clusters joined by 6 extra ZnO pairs, or of 6 $(ZnO)_{14}$ clusters with 6 common ZnO pairs, or of

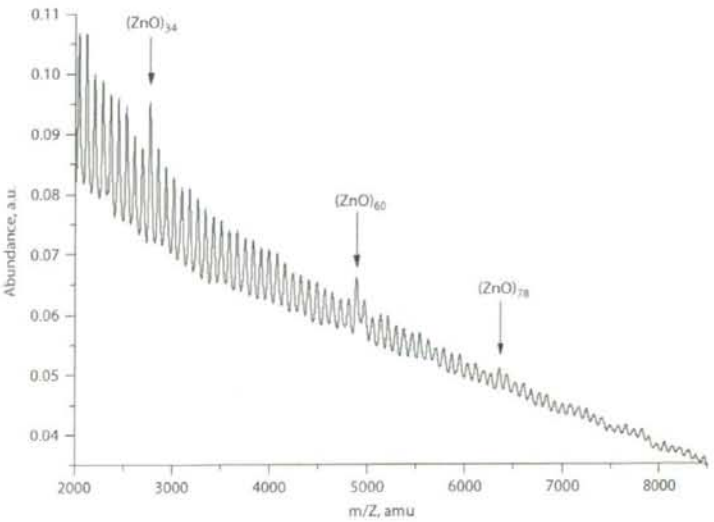

Fig. 1. TOF mass spectrum of ZnO clusters.

6 $(ZnO)_{13}$ clusters which are extremely stable for other II–VI group compounds [10]. Further calculations of the isomers will show the most stable structure for the cluster.

4. Conclusion

Using of ZnO_2 precursor allowed obtaining the mass spectrum of ZnO clusters of up to about a hundred of monomers. The spectrum clearly shows a set of magic clusters neither observed nor predicted hitherto: $(ZnO)_{34}$, $(ZnO)_{60}$ and $(ZnO)_{78}$. It is supposed, that the magic cluster of 34 monomers has the same core-cage structure as $(CdSe)_{34}$ [2] that found commonly for the other II–VI group compounds [10], whilst the magic cluster of 60 monomers most probably has the structure of $(ZnO)_{12}$ @ $(ZnO)_{48}$ nested cage. Results of our extensive first-principles calculations of the proposed cluster structures prove their stability.

The laser ablation method produces ZnO clusters with structures inaccessible yet by other synthesis methods. We believe that our findings of ZnO clusters of enhanced stability will help to develop methods of their production in mass quantities. The enhanced stability of the rather large $(ZnO)_{60}$ cluster may be especially useful for applications, where the atomic precision of about 1 nm scale inorganic semiconductor nanoparticles is necessary.

References

[1] H.W. Kroto, J.R. Heath, S.C. O'Brien, R.F. Curl, R.E. Smalley, C60: Buckminsterfullerene, Nature 318 (1985) 162–163.

[2] A. Kasuya, R. Sivamohan, Yu.A. Barnakov, I.M. Dmitruk, T. Nirasawa, V.R. Romanyuk, et al., Ultra-stable nanoparticles of CdSe revealed from mass spectrometry, Nat. Mater. 3 (2004) 99–102.

[3] E.C. Behrman, R.K. Foehrweiser, J.R. Myers, B.F. French, M.E. Zandler, Possibility of stable spheroid molecules of ZnO, Phys. Rev. A 49 (1994) R1543–R1546.

[4] J.M. Matxain, J.E. Fowler, J.M. Ugalde, Small clusters of II–VI materials: Zn_iO_i, $i = 1$–9, Phys. Rev. A 62 (2000) 053201–053210.

[5] M. Zhao, Y. Xia, Z. Tan, X. Liu, L. Mei, Design and energetic characterization of ZnO clusters from first-principles calculations, Phys. Lett. A 372 (2007) 39–43.

[6] B. Wang, X. Wang, G. Chen, S. Nagase, J. Zhao, Cage and tube structures of medium-sized zinc oxide clusters $(ZnO)_n$ ($n = 24$, 28, 36 and 48), J. Chem. Phys. 128 (2008) 144710.

[7] A. Burnin, J.J. BelBruno, $Zn_nS_n^+$ cluster production by laser ablation, Chem. Phys. Lett. 362 (2002) 341–348.

[8] I.M. Kukreja, A. Rohlfing, P. Misra, F. Hillenkamp, K. Dreisewerd, Cluster formation in UV laser ablation plumes of ZnSe and ZnO studied by time-of-flight mass spectrometry, Appl. Phys. A 78 (2004) 641–644.

[9] S. Wu, N. Yuan, H. Xu, X. Wang, Z. A Schelly, Synthesis and bandgap oscillation of uncapped, ZnO clusters by electroporation of vesicles, Nanotechnology 17 (2006) 4713–4718.

[10] V. Romanyuk, I. Dmitruk, Yu. Barnakov, R. Belosludov, A. Kasuya, Ultra-stable nanoparticles in A_2B_6 (A_2 = Cd, Zn; B_6 = Se, S, Te) compounds, J. Nanosci. Nanotechnol. to appear.

[11] O. Sedo, M. Alberti, J. Janca, J. Havel, Laser desorption—ionization time of flight mass spectrometry of various carbon materials, Carbon 44 (2006) 840–847.

[12] V.V. Pokropivny, V.V. Skorokhod, G.S. Oleinik, A.V. Kurdyumov, T.S. Bartnitskaya, A.V. Pokropivny, et al., Boron nitride analogs of fullerenes (the fulborenes), nanotubes, and fullerites (the fulborenites), J. Solid State Chem. 154 (2000) 214–222.

Cancer Chemother Pharmacol
DOI 10.1007/s00280-008-0882-8

ORIGINAL ARTICLE

Phase II study of capecitabine and trastuzumab combination chemotherapy in patients with HER2 overexpressing metastatic breast cancers resistant to both anthracyclines and taxanes

Takanori Ishida · Takayoshi Kiba · Motohiro Takeda · Kotone Matsuyama · Satoshi Teramukai · Ryota Ishiwata · Norikazu Masuda · Yuichi Takatsuka · Shinzaburo Noguchi · Chikashi Ishioka · Masanori Fukushima · Noriaki Ohuchi

Received: 27 August 2008 / Accepted: 20 November 2008

Abstract
Purpose The purpose of this study was to investigate the activity of capecitabine and trastuzumab in patients with HER2-overexpressing metastatic breast caner resistant to both anthracyclines and taxanes.
Method From June 2003 and May 2006, 40 female patients with measurable or assessable metastatic breast cancer were enrolled and data from 38 patients were reviewed extramurally and analyzed. Patients were treated with weekly trastuzumab given at a dose of 2 mg/kg/day over 90 min (4 mg/kg/day on the first infusion) and capecitabine given at a dose 1,657 mg/m^2/day during 21 days with a subsequent pause of 7 days. This cycle was repeated every 28 days. The primary endpoint was overall survival and secondary endpoints were progression-free survival and response rate.
Result A median of 4.5 cycles (range 1–9 cycles) were delivered. The median age was 53 (range 30–69 years). Median overall survival and progression-free survival was 22.3 and 4.1 months, respectively. Survival rate at 1 and 2 year was 81.6 and 47.4%, respectively. Response rate was 18.4% (95% CI, 7.7–34.3%). All evaluable patients have responded with two CR (5.3%), 5 PR (13.2%), 20 SD (52.6%), 8 PD (21.1%) and 3 NE (7.9%). Regarding the hematological toxicities, grade 1/2/3 neutropenia, grade 1/2 anemia, grade 1 thrombocytopenia and grade 1/2 liver dysfunction were also common. No treatment-related death was reported.
Conclusion The combination of capecitabine and trastuzumab is active and well-tolerated in patients with HER2-overexpressing breast caner resistant to both anthracyclines and taxanes.

Keywords Phase II study · Capecitabine · Trastuzumab · Metastatic breast caner

Abbreviations

BCIRG	Breast Cancer International Research Group
CI	Confidence interval
CMF	Cyclophosphamide, methotrexate and fluorouracil
ECOG	Eastern Cooperative Oncology Group
ER	Estrogen receptor
FU	Fluorouracil

T. Ishida · M. Takeda · N. Ohuchi (✉)
Department of Surgical Oncology,
Tohoku University School of Medicine,
1-1 Seiryo-machi, Aoba-ku, Sendai 980-8574, Japan
e-mail: noriakio@mail.tains.tohoku.ac.jp

T. Kiba · K. Matsuyama · S. Teramukai · R. Ishiwata · M. Fukushima
Translational Research Informatics Center, Kobe, Japan

K. Matsuyama · S. Teramukai · M. Fukushima
Department of Clinical Trial Design and Management,
Graduate School of Medicine, Kyoto University,
Kyoto, Japan

N. Masuda
Department of Surgery, Osaka National Hospital, Osaka, Japan

Y. Takatsuka
Department of Surgery, Kansai Rosai Hospital, Hyogo, Japan

S. Noguchi
Department of Breast and Endocrine Surgery,
Graduate School of Medicine, Osaka University,
Osaka, Japan

C. Ishioka
Department of Clinical Oncology,
Institute of Developing, Aging and Cancer,
Tohoku University, Sendai, Japan

Published online: 12 December 2008